Acta Pharmaceutica Sinica B 2024;14(4):1661−1676

Chinese Pharmaceutical Association
Institute of Materia Medica, Chinese Academy of Medical Sciences

Acta Pharmaceutica Sinica B

www.elsevier.com/locate/apsb
www.sciencedirect.com

ORIGINAL ARTICLE

Single-cell transcriptomics reveals the ameliorative effect of rosmarinic acid on diabetic nephropathy-induced kidney injury by modulating oxidative stress and inflammation

Junhui Chen[a,b,†], Qian Zhang[b,c,†], Jinan Guo[d,†], Di Gu[e,†], Jing Liu[b], Piao Luo[b,c], Yunmeng Bai[b], Jiayun Chen[b,c], Xinzhou Zhang[f,*], Sheng Nie[g,*], Chunbo Chen[h,*], Yulin Feng[a,*], Jigang Wang[a,b,c,i,j,*]

[a]*National Pharmaceutical Engineering Center for Solid Preparation of Chinese Herbal Medicine, Jiangxi University of Chinese Medicine, Nanchang 330006, China*
[b]*Department of Pulmonary and Critical Care Medicine, Shenzhen Institute of Respiratory Diseases, and Shenzhen Clinical Research Centre for Geriatrics, Shenzhen People's Hospital, First Affiliated Hospital of Southern University of Science and Technology, Second Clinical Medical College of Jinan University, Shenzhen 518020, China*
[c]*School of Traditional Chinese Medicine and School of Pharmaceutical Sciences, Southern Medical University, Guangzhou 510515, China*
[d]*Department of Urology, and Shenzhen Clinical Research Centre for Geriatrics, Shenzhen People's Hospital, the First Affiliated Hospital, Southern University of Science and Technology, Shenzhen 518020, China*
[e]*Department of Urology, the First Affiliated Hospital of Guangzhou Medical University, Guangzhou 510230, China*
[f]*Department of Nephrology, Shenzhen Key Laboratory of Kidney Diseases, and Shenzhen Clinical Research Centre for Geriatrics, Shenzhen People's Hospital, the First Affiliated Hospital, Southern University of Science and Technology, Shenzhen 518020, China*
[g]*Department of Nephrology, Nanfang Hospital, the First Affiliated Hospital of Southern Medical University, Guangzhou 510515, China*
[h]*Department of Critical Care Medicine, Shenzhen People's Hospital (the Second Clinical Medical College, Jinan University, the First Affiliated Hospital, Southern University of Science and Technology), Shenzhen 518020, China*
[i]*State Key Laboratory for Quality Esurance and Sustainable Use of Dao-di Herbs, Artemisinin Research Center, and Institute of Chinese Materia Medica, China Academy of Chinese Medical Sciences, Beijing 100700, China*
[j]*Department of Oncology, the Affiliated Hospital of Southwest Medical University, Luzhou 646000, China*

Received 16 October 2023; received in revised form 11 December 2023; accepted 4 January 2024

*Corresponding authors.
E-mail addresses: jgwang@icmm.ac.cn (Jigang Wang), fengyulin2003@126.com (Yulin Feng), gghccm@163.com (Chunbo Chen), niesheng0202@126.com (Sheng Nie), xin.zhou2@qq.com (Xinzhou Zhang).
[†]These authors made equal contributions to this work.
Peer review under the responsibility of Chinese Pharmaceutical Association and Institute of Materia Medica, Chinese Academy of Medical Sciences.

https://doi.org/10.1016/j.apsb.2024.01.003

KEY WORDS

Rosmarinic acid;
Diabetic nephropathy;
scRNA sequencing;
Injury;
Oxidative stress;
Inflammation;
Proteomics

Abstract Diabetic nephropathy (DN) is a severe complication of diabetes, characterized by changes in kidney structure and function. The natural product rosmarinic acid (RA) has demonstrated therapeutic effects, including anti-inflammation and anti-oxidative-stress, in renal damage or dysfunction. In this study, we characterized the heterogeneity of the cellular response in kidneys to DN-induced injury and RA treatment at single cell levels. Our results demonstrated that RA significantly alleviated renal tubular epithelial injury, particularly in the proximal tubular S1 segment and on glomerular epithelial cells known as podocytes, while attenuating the inflammatory response of macrophages, oxidative stress, and cytotoxicity of natural killer cells. These findings provide a comprehensive understanding of the mechanisms by which RA alleviates kidney damage, oxidative stress, and inflammation, offering valuable guidance for the clinical application of RA in the treatment of DN.

1. Introduction

Diabetic nephropathy (DN) is one of the most prevalent microvascular complications of diabetes, accompanying ∼40% of diabetic patients[1,2]. DN causes multiple dysfunctional signal cascades in the kidneys, affecting metabolism, hemodynamics, inflammation and autophagy, ultimately resulting in end-stage renal failure[3,4]. Oxidative stress and inflammation play primary roles in the pathogenesis of DN. Increased oxidative stress in DN is a consequence of imbalance between the production of hyperglycemia-induced ROS and antioxidant defense mechanisms[5]. Moreover, inflammation-related processes are activated in response to hemodynamic or metabolic dysfunctions induced by DN, which leads to the release of various chemokines and pro-inflammatory cytokines such as interleukin-1β (*IL-1β*), interleukin-6 (*IL6*), interleukin-18 (*IL18*) and adhesion molecules (*Vcam1*, *Icam1*)[6,7]. Additionally, immune cells (macrophages and T-lymphocytes) recruited by chemokine signals release additional pro-inflammatory mediators to exacerbate renal inflammation[8,9].

Rosmarinic acid (RA) is a natural phenolic acid[10] known for its ability to reduce oxidative stress by effectively scavenging ROS, and has been reported by multiple studies to exhibit anti-inflammatory properties by modulating NF-κB and MAPK pathways[11–13]. Besides, several reports have shown that the pathogenesis of DN can be alleviated by RA[14,15]. However, the specific mechanism of RA in treating DN is still poorly understood, especially at the single cell level. Advancements in single-cell RNA (scRNA) sequencing technology have allowed for the analysis of cellular heterogeneity and gene expression changes in response to drug treatments in specific cell types of complex tissues[16,17]. Recently, scRNA sequencing has also been used to study mechanisms underlying the therapeutic effects of herbal medicine and natural products[18–20]. In this study, we performed single-cell transcriptome profiling of DN to gain insights into the cell-specific changes following RA treatment. We identified DN-induced changes in expression patterns of oxidative stress-related genes and inflammatory factors (*Il1b*, *Nfkb1*, *Nfkb2*, and *Stat3*), which were subsequently rescued by RA treatment. RA could also alleviate injury in renal epithelial cells. Collectively, our results provide a comprehensive understanding of how RA alleviates renal damage, oxidative stress, and inflammation, thereby offering valuable insights for its clinical application in treating DN.

2. Materials and methods

2.1. Animal experiments

Male C57BLKS/J mice (eight weeks old, weighing 45 ± 5 g) and C57BL/6 mice (eight weeks old, weighing 22 ± 2 g) were procured from Ji-Cui Pharma Biotechnology Co., Ltd., China. The mice were housed in a standard laboratory facility with a 12-h light/dark cycle and maintained at ordinary room temperature. After one week of acclimation, the mice were randomly divided into four groups, with two mice per group. The groups were treated with the following: control, model, 300 mg/kg/day MET (Sino-US Squibb Pharmaceutical Co., Ltd., Shanghai), 100 mg/kg/day RA for a duration of 39 days. Weekly measurements of mouse body weights were taken, and physiological indicators were measured and analyzed using collected blood samples. Urine samples were collected to measure the albumin-to-creatinine ratio (ACR). Upon concluding the experiment, all mice were anesthetized, sacrificed, and kidney tissues were collected for scRNA-seq and histological analysis.

2.2. Biochemical and histological analysis

Several indicators, such as blood urea nitrogen (BUN), creatinine (CRE), aspartate aminotransferase (AST), and alanine aminotransferase (ALT), were assessed using a TOSHIBA biochemistry instrument. For histological analysis, a portion of kidney tissues was embedded in paraffin and sectioned for H&E staining. The H&E staining allowed for the examination of histological morphology and structural changes in the kidney tissues. To assess the extent of inflammation/injury, Masson's trichrome staining was performed. Microscope images were captured to document and analyze the histological and inflammation/injury observed in the kidney tissues.

2.3. Dissociation of single cells from murine kidneys

According to the manufacturer's instructions, kidney samples were dissociated using the Kidney Dissociation Kit (Miltenyi Biotec 130-105-807) on a gentleMACS Dissociator for approximately 30 min. To obtain uniform cell suspensions, the dissociated cells were filtered through a 70 μm strainer into

PBS and subsequently centrifuged at 300×*g* for 10 min at 4 °C. After removing the supernatant, the pelleted cells were suspended in Red Blood Cell Lysis Solution (130-094-183, Miltenyi Biotec, USA). After being washed twice with PBS, the cells were resuspended in sorting buffer (PBS supplemented with 0.04% bovine serum albumin) to achieve a single-cell suspension.

2.4. Single-cell library preparation and sequencing

Following the user's instructions, scRNA-seq libraries were constructed using the Chromium Next GEM Single Cell 3′ Kit v3.1 (PN-1000121, 10 × Genomics, CA, USA). Briefly, approximately 10,000 cells captured in droplets were encapsulated in Gel Beads in Emulsion (GEMs). Transcripts were reverse transcribed, and then the emulsions were broken to collect the cDNA, which was subsequently purified and amplified using SPRIselect reagent (B23318, Beckman Coulter, CA, USA) for PCR. The amplified cDNA was then fragmented and end-repaired. The sequencing library was prepared following the manufacturer's user guide. The library was sequenced on an Illumina NovaSeq 6000 sequencer (Illumina, CA, USA) with 150 bp paired-end reads.

2.5. scRNA-seq quality control and data processing

The raw data underwent filtering to remove low-quality reads and adapter contamination using fastp (version 0.20.0) with default parameters[21]. Subsequently, the high-quality reads were processed with Cell Ranger (version 6.0.1) to generate cell-gene expression matrices by aligning them to the mouse reference genome (mm10) individually (https://github.com/10XGenomics/cellranger). Next, Seurat (version 4.0.4) was employed for a second round of quality control and downstream analysis[22]. Each sample was normalized and scaled using Seurat's SCTransform function separately. The IntegrateData module was applied to integrate the expression matrices of six samples with high-quality cells, resulting in an integrated cells-genes expression matrix devoid of batch effects. Subsequently, Dimensionality reduction was achieved using RunPCA, while Uniform Manifold Approximation and Projection (UMAP) was employed for nonlinear dimensionality reduction and visualization of the datasets.

2.6. Cell type annotation

To annotate cell types, we employed a combination of canonical cell markers and cluster-specific expression genes to validate the identity of each cluster obtained in the two-dimensional space. Seurat's FindAllMarkers function was used to identify cluster-specific expression genes by comparing a certain cluster with the remaining clusters. Initially, we determined the identity of each cluster based on the expression of canonical cell markers. We assigned the cluster to the marker-related cell type if a marker gene exhibited high expression in a specific cluster. On the other hand, if a cluster did not express any canonical marker gene, cluster-specific expression genes were used to identify the cell type of the cluster. Moreover, the identity of clusters exhibiting high expression of classical markers was further confirmed by the cluster-specific expression genes. This combined approach utilizing both canonical cell markers and cluster-specific expression genes provided a robust method for accurately annotating the cell types within each cluster.

2.7. Differentially expressed gene (DEG) and gene functional enrichment analysis

Seurat's FindMarkers function was utilized to identify differentially expressed genes (DEGs) with default parameters. Specifically, we compared DKD with Normal and RA-treated DN (DKD_RA). DEGs were defined as genes with an adjusted *P*-value <0.05 and a $|\log \text{fold change}| > 0.25$. To gain insights into the biological functions associated with the identified DEGs, the clusterProfiler package (version 3.18.1)[23] was used to perform Gene Ontology (GO) enrichment analysis. We separately conducted GO enrichment analysis for the up-regulated and down-regulated DEGs. The enriched GO terms/pathways were filtered based on a Benjamini-Hochberg (BH) corrected *P*-value <0.05. The significant GO terms/pathways were further utilized for downstream analysis and visualization.

2.8. Analysis of gene regulatory network

The analysis of transcription factor activity and gene regulatory network was carried out using the Python implementation of the SCENIC method[24], known as pySCENIC (v0.11.2)[25].

2.9. Cellular crosstalk analysis

CellChat (Version 1.4.0) was used to perform cellular crosstalk analysis based on the ligand−receptor interactions among cell types with default parameters[26].

2.10. Label-free LC−MS/MS detection and data analysis

After obtaining the proteome data, we conducted downstream analysis and visualization using the R programming language. Firstly, we filtered the data to retain proteins that were simultaneously detected in at least three replicates. Then, we applied variance stabilizing transformation (VST) to normalize the data, taking into account the inherent variability in proteome data[27]. Due to the presence of missing values in the proteome data, we employed imputation techniques. Specifically, we used random draws from a Gaussian distribution centered on the minimum value to impute missing values[27]. Next, we utilized the limma package to identify differentially expressed proteins (DEPs)[28]. The *P*-values obtained were adjusted for multiple testing using the fdrtools package[29]. Proteins with an adjusted *P*-value of less than or equal to 0.05 and a $|\text{fold change}| \geq 1.3$ were considered as DEPs, indicating significant changes in protein expression. To elucidate the functions of the DEPs, we performed enrichment analysis using the enrichR package[30]. The analysis involved assessing functional enrichment in terms of Gene Ontology Biological Process 2021 and KEGG 2021 Mouse databases. Functional entries with an enrichment *P*-value less than 0.05 were selected for further downstream analysis and visualization.

2.11. Western blot analysis

Proteins were extracted using pre-chilled RIPA lysis solution (P0013B, Beyotime, China), and their concentrations were measured. Equal amounts of proteins from different samples were loaded onto SDS-PAGE gels for separation. The separated proteins were then transferred onto PVDF membranes (IPVH00010, Millipore, Massachusetts, USA). To prevent non-specific binding, the membranes were blocked with 5% milk at room temperature

for 1 h. Following this, the membranes were incubated with the primary antibodies against interleukin 1 beta (IL-1β, 12442S, CST), nuclear factor kappa B (NF-κB, 10745-1-AP, Proteintech) and glyceraldehyde 3-phosphate dehydrogenase (GAPDH, EM1701-45, HuaBio, China) overnight at 4 °C. After the primary antibody incubation, the membranes were incubated with the corresponding HRP-labeled secondary antibody. The protein bands of interest were visualized using ECL solution (BL523A, Biosharp, China) and semi-quantified using ImageJ software.

2.12. Statistical analysis

Data in this study are representative of at least three independent experiments, and error bars are presented as the mean ± standard error of the mean. *T*-test and One-way ANOVA were employed for statistical analysis of the differences among the groups. Significant *P* values are denoted with asterisks: $^{*}P < 0.05$, $^{**}P < 0.01$, $^{***}P < 0.001$ and ns represented not significant. SCP, pheatmap, and ggplot2 was used for data visualization.

2.13. Data availability

The code used in this study has been submitted to the GitHub repository at https://github.com/Atvar2/DKD-RA. The raw data have been uploaded to the Genome Sequence Archive in the National Genomics Data Center, assigned with the GSA code: CRA012260. These data are publicly accessible at https://ngdc.cncb.ac.cn/gsa.

3. Results

3.1. Single cell profile relating to DN-induced mouse kidney injury and RA treatment

To evaluate the effect of RA on DN, we performed scRNA-seq and proteomics using mass spectrometry techniques on cryopreserved kidney tissues, which were obtained from normal mice (Normal), DN models (DKD) and RA-treated DN (DKD_RA) samples (3 cohorts with 6 samples for scRNA sequencing; 3 cohorts with 9 samples for proteomics analysis). Fig. 1A illustrates the experimental workflow. Following that, samples including Normal, DKD, and DKD_RA were collected for scRNA and proteomics sequencing and downstream analysis. Additionally, the changes of histopathology such as vacuolar deterioration of the tubular epithelium were observed in the kidney tissue of DN mice (Fig. 1B). Notably, DN-induced kidney injury was reduced in part after RA treatment.

The integrated scRNA-seq dataset was processed as described in the methods. After quality control, we obtained a total of 51,882 cells including 17,404 cells from the Normal group, 18,150 cells from the DKD group, and 16,328 cells from the DKD_RA group. The data was dimensionally reduced at 0.8 resolution and visualized in UMAP (Fig. 1C−E and Supporting Information Fig. S1A). To confirm the identities of the 28 obtained cell clusters, we utilized classic marker genes and identified 13 cell lineages (Fig. 1C), including proximal tubule (PT) with high expression of *Slc13a3*, *Slc27a2,* and *G6pc* (which displayed the highest cell ratio of about 73.33% in comparison to other lineages), descending loop of Henle (DLH) with *Aqp1* and *Proser2*, distal convoluted tubule (DCT) with *Emx1*, ascending loop of Henle (ALH) with *Slc12a1* and *Umod*, collecting duct principal cells (CD-PC) with *Aqp2*, *Hsd11b2*, and *Tmem45b*, collecting duct intercalated cells (CD-IC) with *Atp6v0d2* and *Atp6v1g3*, podocytes (Podo) with *Cdkn1c* and *Lamb2*, and endothelium (Endo) with *Flt1* and *Ptprb*. For immune cells, we identified macrophages (Mφ) with high expression of *C1qa*, *C1qb*, and *Lyz2*, neutrophils (Neutro) with *S100a8* and *S100a9*, T cells and NK (T/NK) with *Cd3d* and *Nkg7*, and B cells (B) with *Cd79a* and *Cd79b* (Fig. 1C and D). Notably, we discovered a cell type with high expression of *Cdca3*, *Mki67*, and *Stmn1*, which has been identified as a novel cell type in a published study[31]. Moreover, projecting the expression of these genes on UMAP further suggested cell lineage specificity, consistent with the unique transcription profile of marker genes from each cell type (Fig. S1B and S1C). Correlation analysis revealed high correlation coefficients among the annotated cell types in our single-cell RNA data and corresponding datasets from published single-cell RNA or bulk RNA sequencing studies[31,32] (Fig. S1D and S1E), indicating strong evidence for the correct assignment of cell types.

Next, compared with the Normal group, the percentage of PT increased in DKD from 63.78% to 76.26% (Fig. 1F), consistent with the proliferation of proximal tubular cells during diabetes[33]. For a subset of lineages including ALH, CD-PC, CD-IC and Podo, the proportion decreased in the DKD group, while RA treatment could partially rescue this decrease (Fig. 1F and G). These results show the distributed changes of cells induced by DN including an increase in the proportion of proliferative cells and reductions in certain epithelial cells, which were partially recovered after RA treatment.

3.2. Cellular heterogeneity in response to RA treatment

To uncover the molecular mechanisms behind these cellular changes, Seurat's FindMarker was utilized to identify differentially expressed genes (DEGs) for each cell type. According to the distribution pattern of up- or down-regulated DEGs detected in the two comparisons DKD *vs*. Normal and DKD_RA *vs*. DKD (Supporting Information Fig. S2A and S2B), we observed the expression profiles of DEGs from immune cells, particularly Mφ, revealing significant changes (Fig. S2C−S2G). Notably, our analysis showed that PT exhibited the highest number of DEGs after RA treatment, followed by ALH (as depicted in Fig. S2H). Moreover, the majority of DEGs were primarily found within a single cell type (Fig. S2G and S2H), underscoring cellular heterogeneity in response to RA treatment. Intriguingly, PT showed the largest number of rescued genes by RA treatment followed by ALH, while no rescued genes were identified in Neutro, B, and Podo cells (Fig. 2A). Additionally, we observed several rescued genes, such as *Atox1*, *Abca1*, *Nfkb1*, and *Il1b*, involved in oxidative stress and inflammation (Fig. 2A and B). Functional pathways associated with inflammation, including TNF-α signaling *via* NF-κB, oxidative phosphorylation and apoptosis, were enriched in the genes rescued by RA treatment (Fig. 2C). Next, we found that Podo, DLH, and PT had higher module scores for response to oxidative stress than other cells, while Neutro and Mφ had higher scores for response to inflammation, as shown by the expression pattern of the most variable genes involved in the two processes with higher abundance in the DKD group (Fig. 2D and E).

Collectively, we revealed the cellular heterogeneity in response to RA treatment that regulates the expression of genes involved in oxidative stress and inflammation. Podo and Neutro had the highest module scores for oxidative stress and inflammation, respectively.

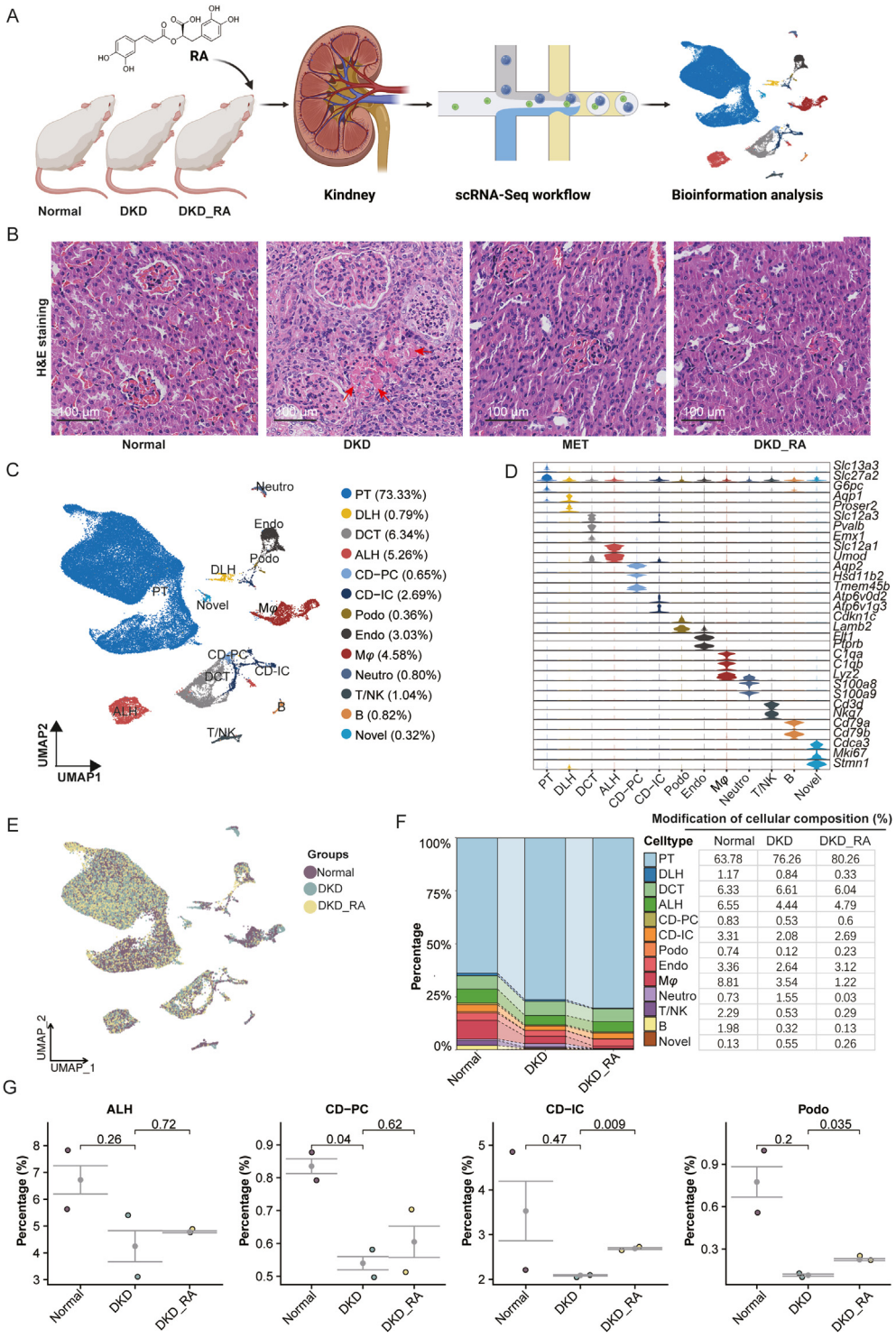

Figure 1 Experimental pipeline and single cell landscape of RA treatment in DN mice. (A) Experimental scheme and workflow diagram in the study (Created with BioRender.com). (B) H&E staining displaying pathological changes of murine kidney in Normal, DKD, and DKD_RA. Scale bar = 100 μm (Red arrows indicating vacuolar deterioration of the tubular epithelium; MET, metformin). (C) Cell types of sequencing cells projecting on UMAP visualization. PT, proximal tubule; DLH, descending loop of Henle; DCT, distal convoluted tubule; ALH, ascending loop of Henle; CD-PC, collecting duct principal cell; CD-IC, collecting duct intercalated cell; Podo, podocyte; Endo, endothelium; Mφ, macrophage; Neutro, neutrophils; T/NK, T cells and NK cells; B, B cells. The percentages in the brackets represent percentage of each cell type. (D) Violin plot displaying expression of classical marker in responding cell type. The *Y*-axis shows the logscale normalized reads count. (E) UMAP visualization showing the group attribute of cells. (F) Bar plot depicting cellular composition in the three groups (Normal, DKD, and DKD_RA). The table beside the bar plot contains the specific percentages. (G) Statistical analysis of cellular changes in ALH, CD-PC, CD-IC, and Podo within Normal, DKD, and DKD_RA.

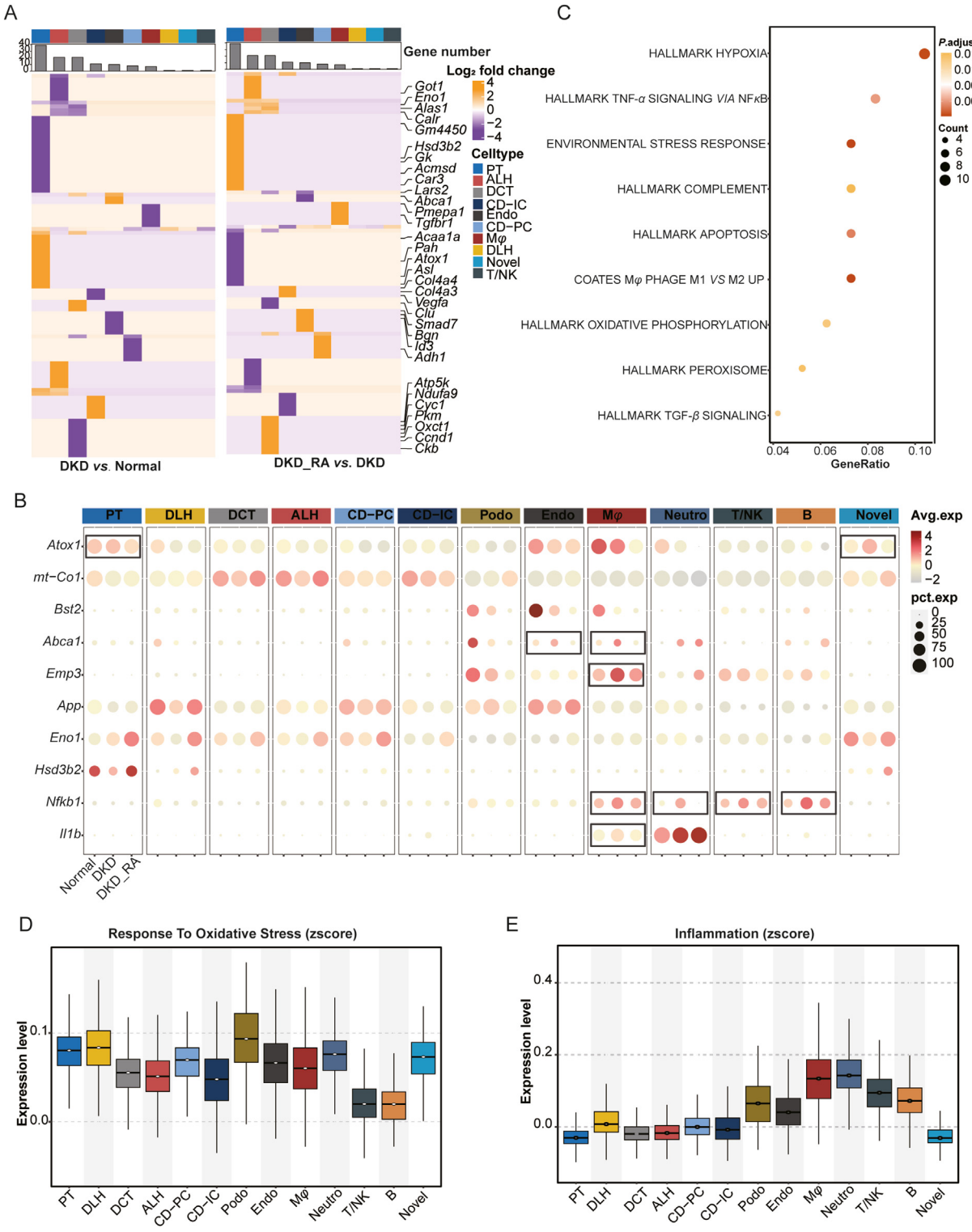

Figure 2 Analysis of differential gene expression and cellular heterogeneity response to RA treatment. (A) Heatmap of $\log_2$ (fold change) of rescuing genes in 13 cell type (left: DKD *vs*. Normal; right: DKD_RA *vs*. DKD). Gene symbols beside heatmap representing genes relating to inflammation and oxidative stress. (B) Expression levels of up-regulating genes in the DKD group, which display significant variability among cell types. Rectangle marking genes that significantly upregulated in the certain cell type. (C) Dot plot displaying pathway enrichment of rescuing genes. (D) Distribution of response to oxidative stress module score in identifying cell types. (E) Distribution of inflammation module score in identifying cell types.

3.3. RA treatment relieves PT S1 cell injury induced by DN

The proximal tubule (PT), which is densely packed with mitochondria and relies on oxidative phosphorylation, constitutes the majority of the kidney parenchymal cells and is prone to damage from oxidative, hypoxic and metabolic stressors, contributing to the progression of diabetic renal disease[34,35]. To investigate the potential mechanism of PT in the DKD group, we performed enrichment analysis for PT-related DEGs and found that these genes were mainly enriched in metabolic processes and oxidative stress-related pathways, such as the small molecule catabolic process, urate metabolic process, reactive oxygen species metabolic process, oxidative phosphorylation, and cellular response to hypoxia (Fig. 3A). In detail, we re-clustered PT cells into 12 clusters, assigning identities based on classical markers and obtained three subtypes (namely S1, S2, and S3), each with a specific expression pattern (Fig. 3B and C). S1 and S3 segments were characterized by the expression of their corresponding markers, while the marker genes of S2 (*Fxyd2*, *Mif,* and *Gsta2*) were also expressed in the other segments, representing the transitional state of PT (Fig. 3D)[17,31]. Moreover, the composition of S2 segment increased in the DKD group compared with Normal mice, and this increase was partially reversed after RA treatment. The opposite trend was observed in S1 (Fig. 3E).

Further analysis found that injury markers (*C3*, *Myc*, *Dcdc2a,* and *Sema5a*)[17,36] were mainly enriched in S1 and S3, in line with the high inflammation scores of the two subtypes compared with S2 (Fig. 3F and G and Supporting Information Fig. S3A). Subsequently, we computed the injury scores based on the injury markers outlined by Kirita Y et al. in their PNAS (2020) study and mapped these scores onto the UMAP[36]. Intriguingly, PT S1 exhibited the highest injury score, as depicted in Fig. S3B. To further delve into the details of inflammation, we projected the inflammation scores onto the UMAP. The results indicated that PT S1 displayed a higher inflammation score in contrast to the other two segments at the single-cell level (Fig. S3C). However, the scores of oxidative stress gene set sourced from the MGI database (https://www.informatics.jax.org/) appeared relatively consistent across all three subtypes (Fig. S3D). Notably, the injury score of S1 with the highest inflammation scores were remarkably increased in the DKD group, while RA treatment significantly reversed this trend in agreement with the proteomics results (Fig. 3H and I). Therefore, we investigated the expression pattern of genes involved in oxidative stress, wound repair, and inflammation in the three groups for S1 (Fig. 3J, Fig. S3E) and detected that RA treatment alleviated the expression of oxidative stress genes, such as *Atox1*, *Gpx1*, *Chchd2*, *Txnip*, *Ndufs2*, *Sod2*, *Mgst1*, *Gas5*, *Cat*, *Vnn1,* and *Prdx1*, as well as wound repair genes (*F13a1*, *Entpd1*, *Fga*, *Dysf*, *Fgg*, and *Ccr1*). Furthermore, the expression of pro-inflammatory genes such as *Cd8a*, *Csf3r*, *Nkg7*, *Il1b*, *Cd14*, and *Ccr7* were diminished following RA treatment (Fig. S3E). Moreover, according to the prediction of transcription factors (TF) regulatory activity, we identified that pro-inflammatory TFs (*Rara*, *Xbp1*, *Bcl3*, *Nfkb2*, *Hif1a*, *Fosl2*, and *Stat3*) were activated in the DKD group, while their activity scores were decreased by RA treatment (Fig. 3K). Overall, RA treatment could improve PT S1 injury induced by DN by regulating wound repair, oxidative stress and inflammation.

3.4. RA treatment improves podocytes injury in DN mouse

To investigate the effect of RA treatment on the other epithelial segments, we re-clustered these nephron cells into 9 subtypes with cluster-specific marker genes, including DLH, DCT1, DCT2, ALH, CD-PC, A-IC, B-IC, CD-Trans, and Podo (Fig. 4A and B). The ratios of ALH, B-IC, and Podo decreased while those of the DCT2, A-IC, and CD-PC subtypes distinctly increased in the DKD group. RA treatment slightly reversed the ratio changes of these segments compared with DKD (Fig. 4C, Supporting Information Fig. S4A).

Additionally, we performed enrichment analysis of DEGs identified in these cells and found that the up-regulated DEGs in the DKD group compared to the Normal group were mainly enriched in inflammatory processes, such as regulation of inflammatory response, interleukin-6 production and reactive oxygen species metabolic process, and pathways related to migration or proliferation of immune cells (Fig. S4B). In the comparison of DKD_RA to DKD, the upregulated genes were mainly enriched in processes associated with ATP metabolic process, glucose metabolic process and oxidative stress response, and negative regulation of apoptotic signaling (Fig. S4C).

Next, we examined the expressed distribution of injury marker genes (*Vcam1*, *C3*, *Cp*, *Lcn2*, and *Clu*) across all segments, which suggested the heterogeneous expression of injury genes (Fig. 4D). Particularly, *Clu* showed significant expression across all subtypes, while *Vcam1*, *C3*, *Cp*, *Lcn2*, and *Clu* displayed high expression levels in Podo. Notably, Clusterin (*Clu*) has demonstrated the ability to prevent complement-induced cellular damage in membranous glomerulonephritis, and study have indicated its upregulation in glomerular of patients with DN[37,38]. Vascular cell adhesion protein 1 (*Vcam1*) and Lipocalin-2 (*Lcn2*) have been identified as biomarkers for renal injury[39,40]. *C3a*, associated with complement activation (C3), has been suggested to participate in promoting podocyte damage[41], while Ceruloplasmin (Cp) has been observed to exhibit increased excretion in individuals with impaired glucose tolerance and diabetes[42]. To further evaluate DN-induced injury among these segments, we calculated the inflammation and injury module scores for these segments. Consistent with the expression distribution of injury marker genes, the results showed that Podo had the highest inflammation and injury scores among these subtypes (Fig. 4E). Thus, we evaluate the effect of RA treatment on Podo, we performed enrichment analysis for DEGs of Podo firstly. Our findings detected upregulation in the regulation of inflammatory response, cytokine-mediated signaling pathways, regulation of cell−cell adhesion, cell chemotaxis, myeloid leukocyte migration, wound healing, and the ERK1 and ERK2 cascade in the DKD *vs*. Normal comparison. Conversely, these pathways were downregulated in the DKD-RA *vs.* DKD (Fig. 4F). As predicted in the results, pathways including inflammation, oxidative stress, wound healing, and PI3K-Akt signaling pathway from DEPs results were upregulated in DKD group while downregulated in DKD_RA group (Fig. 4H). Moreover, we found RA treatment reduced the expression of genes involved in cell chemotaxis, oxidative stress, and injury in the Podo subtype (Fig. 4G).

Collectively, we observed heterogeneous responses to injury among these epithelial segments in the DKD group, and RA treatment was able to ameliorate the injury of Podo by regulating cell chemotaxis and oxidative stress.

3.5. RA treatment alleviates inflammation and reduces the recruitment of S100a4 macrophages

Macrophages display notable plasticity, enabling them to adjust their functions based on signals from the local microenvironment

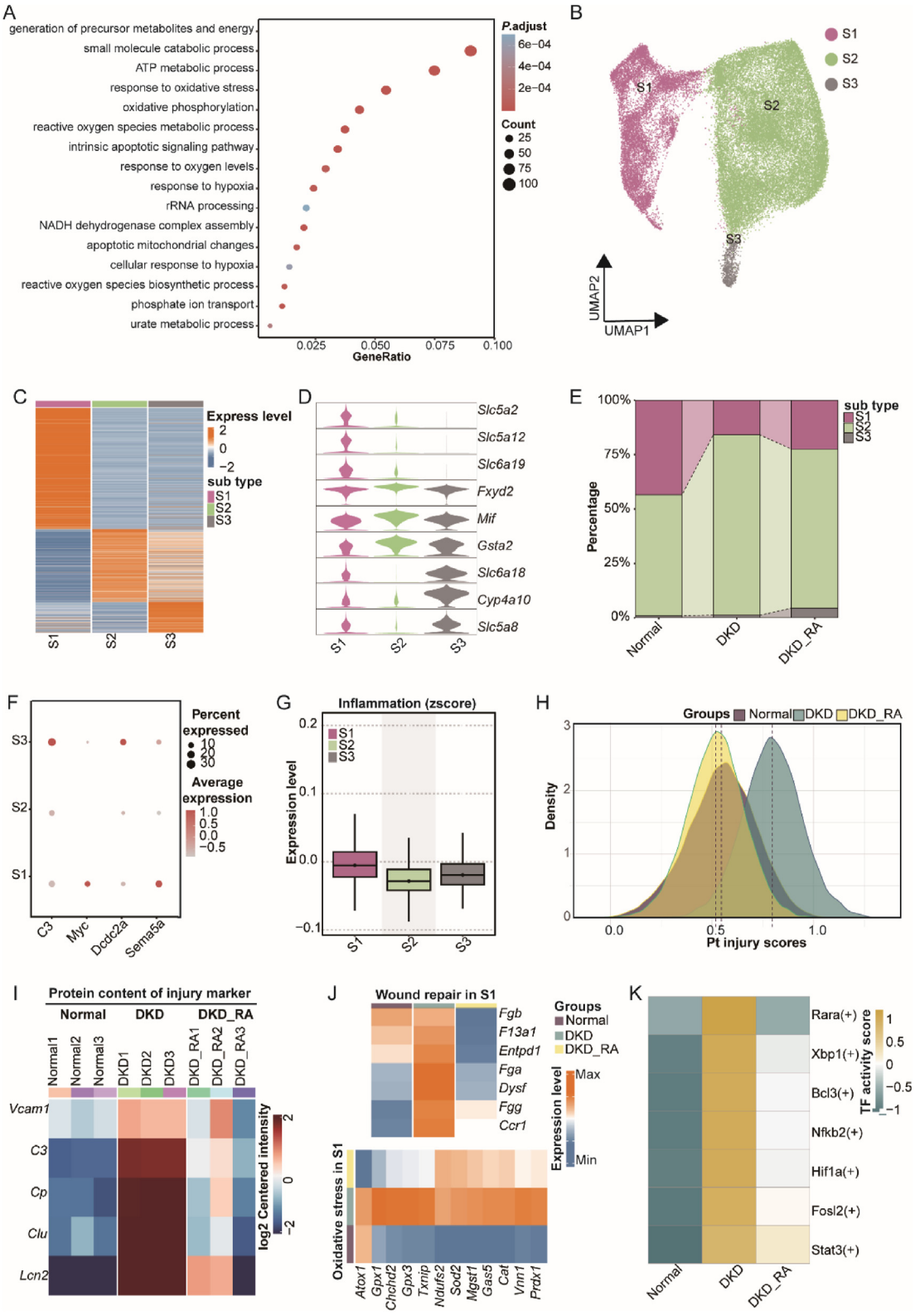

Figure 3 RA treatment relieves PT S1 cell injury induced by DN. (A) Function enrichment of DEGs in PT cells. (B) Re-clustering of PT cells (dividing into PT S1, S2, and S3). (C) Heatmap of average expression of specific expressed genes in each subtype. (D) Violin plot displaying the expression of canonical markers. (E) Cellular composition of three subtypes in Normal, DKD, and DKD_RA. (F) Expression levels of injury marker genes in each subtype. (G) Distribution of inflammation module score in each subtype. (H) Distribution of injury scores in Normal, DKD, and DKD_RA groups. (I) Protein content of injury genes in Normal, DKD, and DKD_RA groups. (J) Heatmap of average expression of genes in S1. Top panel representing genes relating to wound repair; bottom panel showing genes involving in oxidative stress. (K) Heatmap of TF activity in PT S1 within Normal, DKD, and DKD_RA groups.

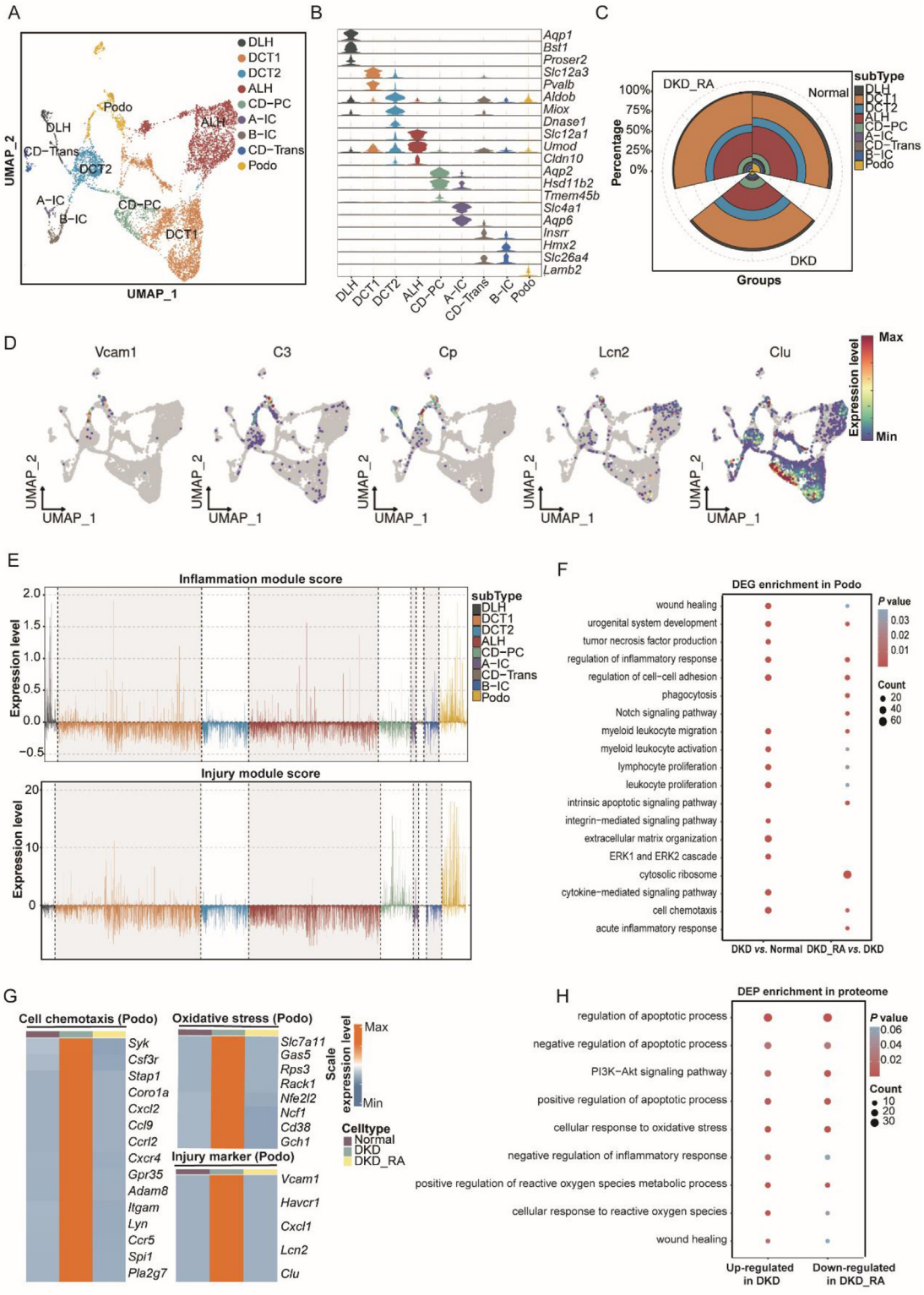

Figure 4 RA treatment improves podocytes injury in DN mouse. (A) Re-clustering of other epithelial segment, revealing nine subtypes: DLH, DCT1, DCT2, ALH, CD-PC, A-IC, B-IC, CD-Trans, and Podo. (B) Violin plot representing expression levels of canonical markers. (C) Cellular composition of the other epithelial segment in Normal, DKD, and DKD_RA. (D) Expression of injury genes projecting UMAP. (E) Distribution of inflammation and injury module scores in the other epithelial segment. Top panel representing inflammation module score; bottom panel showing injury module score. (F) Bubble plot showing the enrichment pathways of up-regulated genes in Podo subtypes in DKD *vs.* Normal and DKD_RA *vs.* DKD. (G) Heatmap showing the expression levels of genes associated with cell chemotaxis, oxidative stress, and injury genes. (H) Bubble plot depicting the enrichment pathways of up-regulated proteins in DKD and down-regulated proteins in DKD_RA.

and recruit additional macrophages in response to inflammatory signals or antigen processing[43]. In this part, we re-clustered macrophages from our data sets and identified four subtypes (Gpx3+Mφ, Cd86+Mφ, S100a4+Mφ, and Cd163+Mφ), each characterized by a unique expression pattern (Fig. 5A and Supporting Information Fig. S5A). Cd86+Mφ was identified as an M1-like macrophage phenotype by the subtype-specific *Cd86*, while Cd163+Mφ with the M2-like phenotype displayed high expression levels of anti-inflammatory markers, such as *Cd163*, *Clec10a,* and *Cd209g*. Hypoxia-inducible as well as inflammation-related genes (*S100a4*, *Anxa2,* and *Il1b*) were enriched in S100a4+Mφ (Fig. 5B). Finally, processes associated

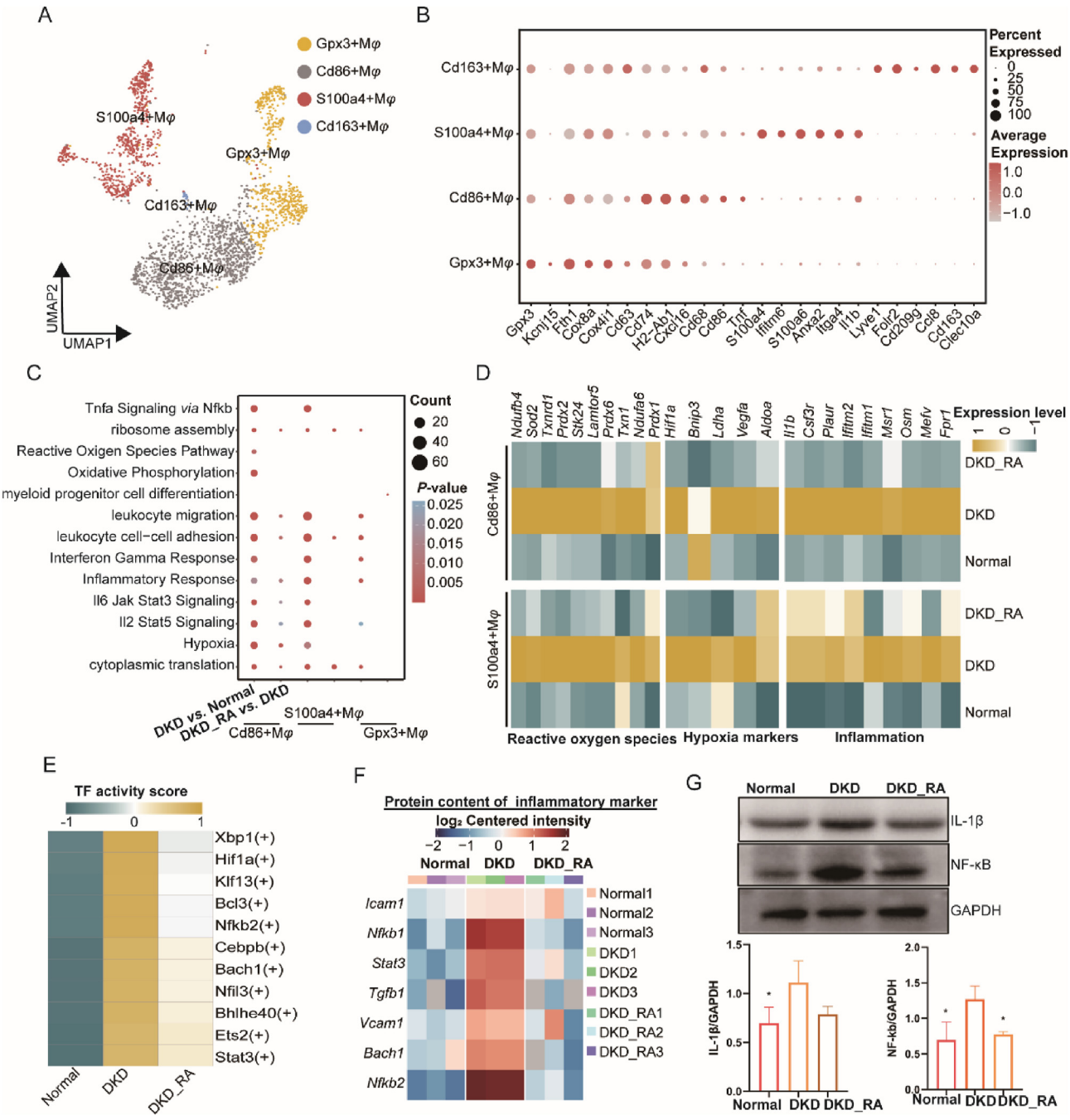

Figure 5 RA treatment alleviates inflammation and reduces the recruitment of *S100a4* macrophages. (A) Re-clustering of macrophage, dividing into four sub types, namely Gpx3+Mφ, Cd86+Mφ, S100a4+Mφ, and Cd163+Mφ. (B) Dot plot showing the expression of subtype-specific genes. (C) Bubble plot displaying pathway enrichment of differentially expressed genes in each subtype of macrophage in DKD *vs.* Normal and DKD_RA *vs.* DKD. (D) Expression level of genes relating to reactive oxygen species, hypoxia and inflammation in Cd86+Mφ and S100a4+Mφ. (E) Heatmap of TF activities in S100a4+Mφ within Normal, DKD, and DKD_RA groups. (F) Protein content of inflammatory genes in Normal, DKD, and DKD_RA. (G) Western blotting and quantitative statistics of proinflammatory factors IL-1β and NF-κB proteins. **P*-value <0.05.

with leukocyte migration-related processes and endocytosis were enriched in Cd86+Mφ, S100a4+Mφ, and Cd163+Mφ. Notably, the process of antigen processing and presentation was specific to Cd86+Mφ (Fig. S5B). We then calculated the alteration of cellular composition for each subtype and found that the proportion of Cd86+Mφ and S100a4+Mφ respectively decreased and increased in the DKD group compared with the Normal group, with both trends being reversed after RA treatment (Fig. S5C).

Next, we performed enrichment analysis on DEGs between two comparisons (DKD *vs*. Normal and DKD_RA *vs.* DKD) across each subtype. DEGs in Cd86+Mφ and S100a4+Mφ were mainly enriched in inflammation processes in DKD, such as Il2 Stat5 signaling, Il6 Jak Stat3 signaling, and TNF-α signaling *via* NF-κB, while RA treatment reduced these inflammation-related responses (Fig. 5C). Moreover, signals or genes associated with reactive oxygen species, hypoxia, and inflammation were significantly downregulated after RA treatment in Cd86+Mφ and S100a4+Mφ, suggesting that RA treatment could ameliorate inflammation and ROS (Fig. 5C, D and Fig. S5D). Activity scores of inflammation-related TFs, such as *Hif1a, Nfkb2,* and *Stat3* were also improved by RA treatment (Fig. 5E), consistent with the expression levels of the corresponding genes and proteins (Fig. 5F). Western blot analysis further confirmed the anti-inflammatory effects of RA treatment (Fig. 5G).

Overall, our findings demonstrate that RA treatment could reduce the recruitment of S100a4+Mφ, reverse the high expression levels of pro-inflammatory and ROS-related genes in DKD, and alleviate inflammation in the Cd86+Mφ and S100a4+Mφ subtypes.

3.6. *RA treatment ameliorates immune dysfunction in DN mice*

Lymphocyte T, B cells and natural killer (NK) cells play critical roles in innate and adaptive immunity. We re-clustered the immune cells from our data set and obtained eight subtypes (namely T_C1, T_C2, T_C3, T_C4, B_C1, B_C2, B_C3, and NK) based on classic markers (T cells: *Cd3d* and *Il7r*; B cells: *Cd79b* and NK: *Ncr1* and *Nkg7*) and cluster-specific genes (Fig. 6A and B). Among them, T_C1, T_C2, and T_C3 exhibited CD8 signature with the expression of *Cd8b1*. Interestingly, the percentages of T_C1 and T_C2 increased in the DKD, while decreased in the DKD_RA group. Conversely, T_C3 exhibited the opposite trend (Fig. 6C). Additionally, we observed distinct changes in the proportions of B_C1 and NK cells of DKD mice that were subsequently reversed by RA treatment, while remaining subtypes exhibited minor changes (Fig. 6C). Furthermore, the highest cytotoxic and inflammatory module scores were displayed in NK cells across all subtypes (Fig. 6D and E; Supporting Information Fig. S6A and S6B). RA treatment effectively improved the cytotoxic and inflammatory response of NK cells in DKD compared with DKD_RA group (Fig. 6F) and diminished the expression of inflammation related genes including *Cd48*, *Cd69*, *Cxcr6*, *Ccl5*, and others in NK cells (Fig. S6C and S6D). Previous studies have reported that *Cd48* and *Cd69* are involved in DN[44,45]. Next, we observed that up-regulated genes in NK cells were enriched in cytokine-mediated signaling pathways and positive regulation of immune responses following RA treatment. Conversely, down-regulated genes were enriched in apoptotic processes, negative regulation of T cell proliferation, and regulation of cell adhesion (Fig. 6G).

Overall, our study reveals the recruitment of NK cells in the DN mice, which enhanced the cytotoxic and inflammatory responses, while RA treatment ameliorated the immune dysfunction induced by DN and remodeled the immune processes of NK cells.

3.7. *RA mediated intercellular crosstalk in murine kidneys with DN*

To investigate the effect of RA treatment on the intercellular interactions of DN in murine kidneys, we evaluated cellular communication among various cell types and subtypes using potential ligand−receptor (LR) pairs[26,46]. We found widespread crosstalk among cell types in the Normal, DKD, and DKD_RA groups (Supporting Information Fig. S7A). Notably, subtypes of kidney epithelium for instance PT S1, Podo, and CD-PC and immune cells such as Cd86+Mφ, S100a4+Mφ, and NK exhibited increased crosstalk strength in the DKD cohort, whereas the crosstalk strength diminished after RA treatment. To explore cellular communication of critical cell types in detail, we examined signals originating from M1-like macrophage Cd86+Mφ, S100a4+Mφ, NK, PT S1, and Podo. Intriguingly, compared with Normal cohort, signals from S100a4+Mφ increased between S100a4+Mφ and CP-PC, Neutro, NK, T_C2, and TC_3 in the DKD group (Fig. 7A). In line with this result, intercellular crosstalk was enhanced between Cd86+Mφ and T_C2, T_C3, NK, and Neutro (Fig. S7B). Moreover, the DN microenvironment increased cellular communication between NK cells and inflammatory cell subtypes Neutro, Cd86+Mφ, and S100a4+Mφ (Fig. 7B), indicating that DN caused intercellular crosstalk dysfunction mainly involving in M1-like macrophages, NK, Neutro, and subtypes of T cells. As depicted in Fig. 7A and B; Fig. S7B, RA treatment could reduce intercellular crosstalk and remodel the intercellular microenvironment. On the other hand, we observed that PT S1 demonstrated a higher injury and inflammation score than other segments of PT (Fig. S3B and S3C). While DN enhanced the crosstalk of PT S1 with M1-like macrophages and NK (Fig. S7C). However, no significant changes were observed in the interaction of Podo with the remaining cell types (Fig. S7D).

Furthermore, we identified specific ligand−receptor (LR) pairs and pinpointed 10 significant LR pairs ($P < 0.01$) (Fig. 7C). The communication probabilities of *Cd274-Pdcd1*, *Cd86-Ctla4,* and *Mif-*(*Cd74*+*Cd44*) pairs in the intercellular communication of Cd86+Mφ, S100a4+Mφ, and NK with subtypes of T cells (T_C1, T_C2, and T_C3) increased in the DKD group. The *Cd274/Pdcd1* pathway, along with *Cd86/Ctla4*, represents crucial immunosuppressive checkpoints playing a pivotal role in suppressing the immune response[47,48]. Studies have indicated that the *Mif/Cd74/Cd44* axis is involved in upregulating PD-L1 levels[49,50]. These findings suggest that the immune response is suppressed in DN. Importantly, our observations indicate that RA may alleviate immunosuppression by down-regulating the communication probabilities. Additionally, the interaction of between up-regulated chemokines and their respective receptors, for instance *Ccl6-Ccr2*, *Ccl5-Ccr5*, *Ccl3-Ccr5*, and *Ccl2-Ccr2*, was upregulated in the intercellular crosstalk of Cd86+Mφ, S100a4+Mφ, and NK with T_C1, T_C2, and T_C3 in the DKD group. Previous studies have characterized *Ccl2*, *Ccl3*, *Ccl5*, and *Ccl6* as pro-inflammatory chemokines[51]. Our results suggest that RA may inhibit inflammation of DN by down-regulating the communication of LR pairs.

4. Discussion

DN, a metabolic disease, promotes a persistent hyperglycemic environment, resulting in heightened free radicals and overproduction of ROS[52,53]. Oxidative stress induced by an imbalance

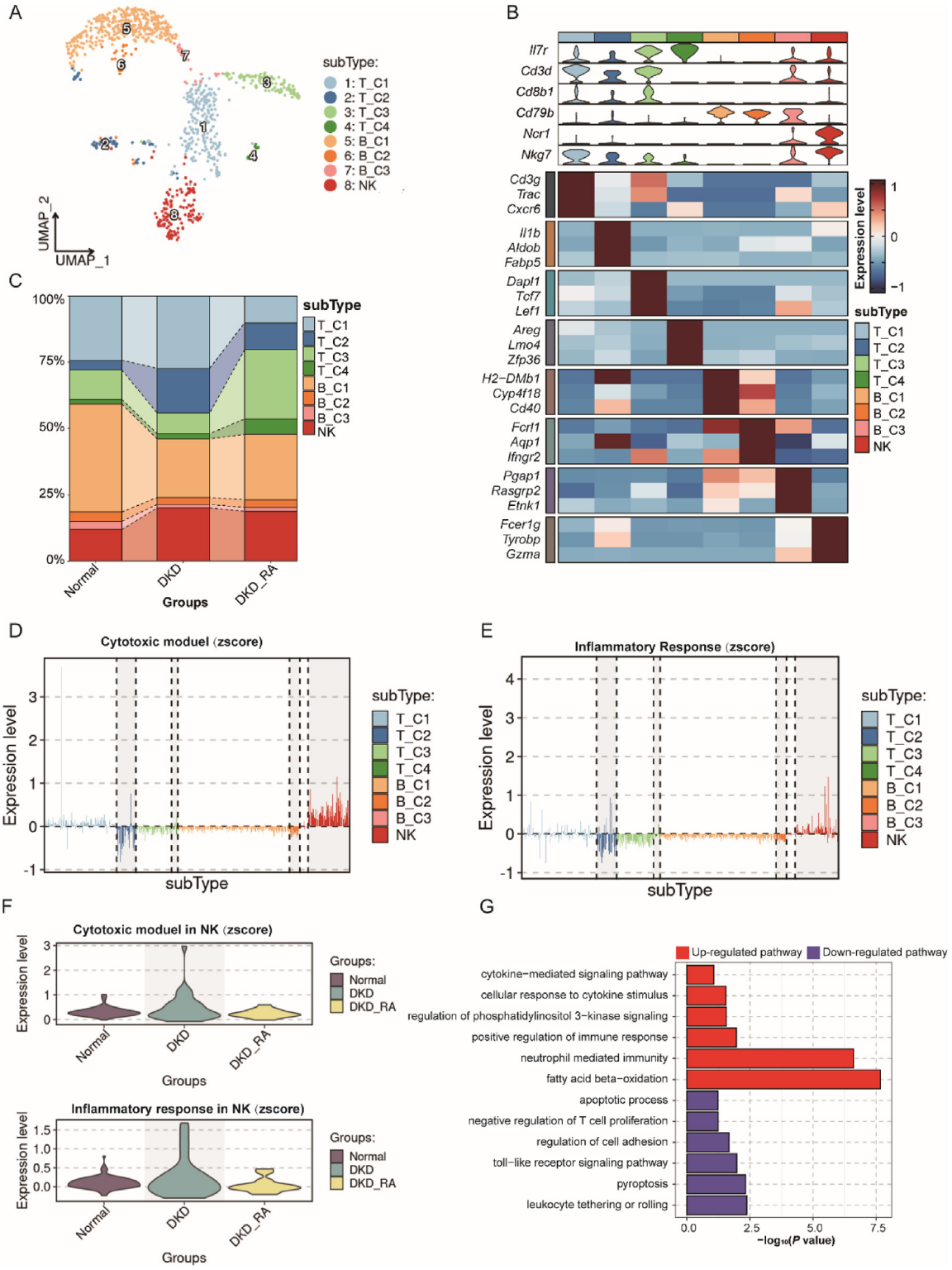

Figure 6 RA treatment ameliorates immune dysfunction in DN mice. (A) The UMAP visualization displaying re-clustering of T lymphocyte, B lymphocyte, and NK cells, revealing 8 subtypes namely T_C1, T_C2, T_C3, T_C4, B_C1, B_C2, B_C3, and NK. (B) Heatmap showing expression levels of top 3 subtype specific markers. Top panel violin plot displaying the expression level of canonical markers of T lymphocyte, B lymphocyte, and NK cells. (C) Cellular composition of subtypes in Normal, DKD, and DKD_RA groups. (D) Distribution of cytotoxic module score in eight subtypes. (E) Distribution of inflammatory response module score in eight subtypes. (F) Expression of cytotoxic module and inflammatory response module in NK cells. The top panel represents the cytotoxic module score, and bottom panel represents the inflammatory response in NK cells. Colors indicate experimental groups (Normal, DKD, and DKD_RA). (G) Pathway enrichment of up-regulated and down-regulated genes of NK cells in DKD_RA *vs*. DKD.

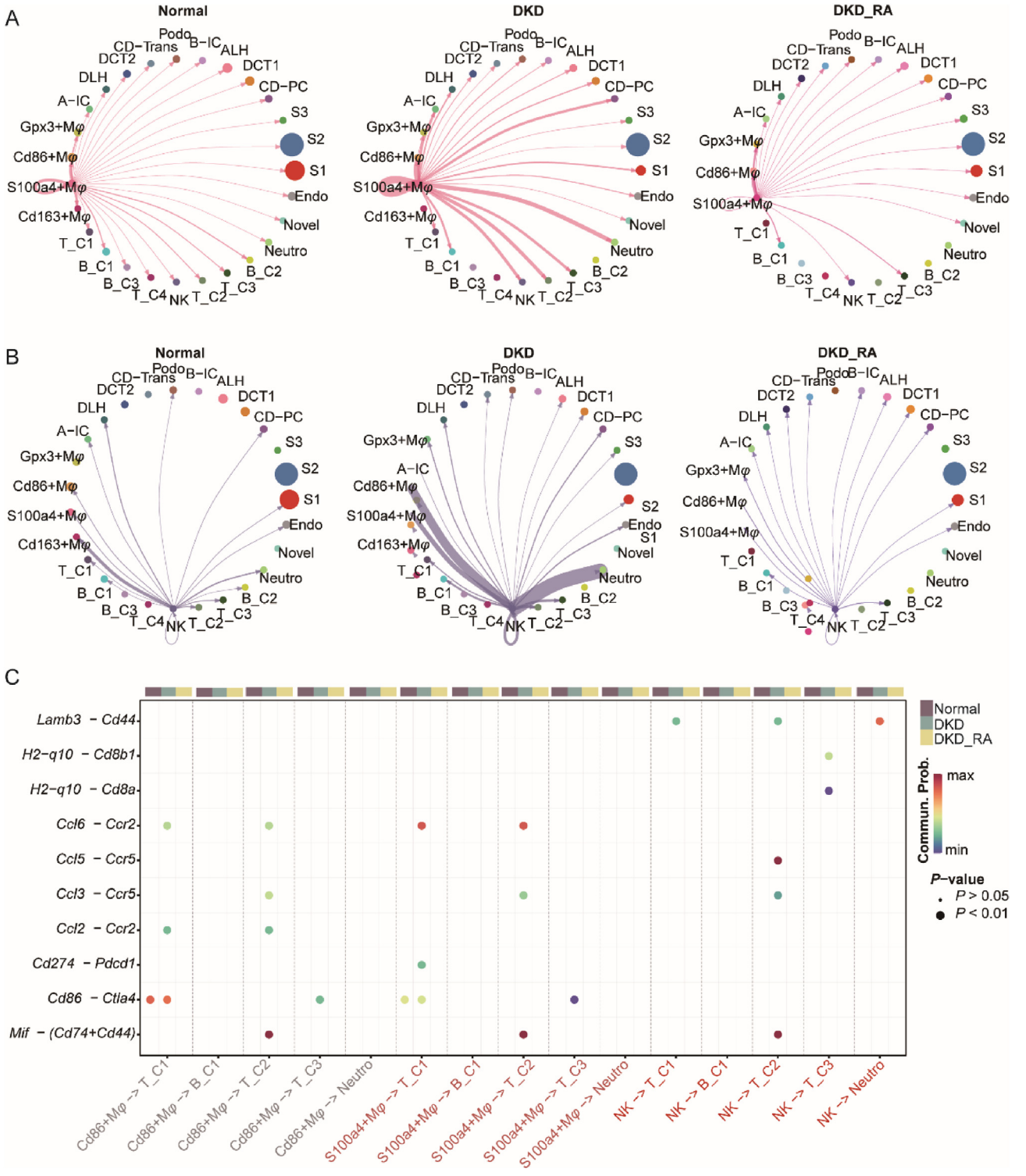

Figure 7 RA mediated intercellular crosstalk in murine kidneys with DN. (A) Chordal graph illustrating the differential interactions between S100a4+Mφ and other cell types in Normal, DKD, and DKD_RA. (B) Chordal graph illustrating the differential interactions between NK cells and other cell types in Normal, DKD, and DKD_RA. (C) The bubble plot displaying the communication probability of ligand-receptor pairs between S100a4+Mφ, Cd86+Mφ and NK cells and other immune cells. The top panel representing the Normal, DKD, and DKD_RA groups.

between the generation of ROS and the presence of antioxidant compounds, and inflammation which has been identified as a key contributor to the development of DN share a close relationship and have the potential to further cause tissue damage, such as the pathogenesis of diabetic nephropathy[54,55]. To investigate the mechanism of RA treatment after DN, we built a single cell map from samples in DKD model groups with or without RA treatment. As displayed in our results, the proportion of epithelial and

immune cells altered significantly in DKD compared with the Normal group, while RA treatment could partially reverse these changes. Additionally, RA decreased oxidative stress and inflammatory response in the DKD group.

The renal tubular structure constitutes the major part of kidney medulla and is sensitive to stimuli from metabolic disorders, hypoxia, and toxins[56,57]. As the predominant renal tubular cell type, the proximal tubule (PT) plays a crucial role in filtering bicarbonates, glucose metabolism, and regulating gluconeogenesis, and is susceptible to injury. The PT is further classified into S1, S2, and S3 segments based on location and morphology, with the S1 segment positioned closest to the glomerulus compared to the other segments[58]. Sodium-glucose cotransporter-2 inhibitors (SGLT2i), used to treat DN, have demonstrated a direct impact on PT S1 by targeting *Slc5a2*[59]. In our study, we observed that PT S1 exhibited higher inflammation and injury scores. Accumulated data have highlighted the critical role of inflammation in the development of DN[60], where a persistent inflammatory response caused tissue damage. RA treatment effectively reduced injury in PT S1, ameliorating inflammation and oxidative stress. Genes related to oxidative stress, such as *Gas5*, promoting inflammation and oxidative stress[61] and the activity of inflammation-related transcription factors (HIF1A, NFKB2, and STAT3)-in PT S1 cells, were highly expressed or increased in the PT of DKD group but were reversed by RA. In addition, we found the proportion of PT S1 was reduced, and the increased part of PT was mainly contributed by S2 in the DKD group. Following RA treatment, the percentage of PT S1 cells increased.

Podocytes, which are a type of glomerular epithelial cells, play an important role in the regulation of glomerular filtration[62]. We found multiple pathological changes in Podo during DN including inflammation, oxidative damage and the increased activity of oxidative stress-related genes, which resulted in decreased glomerular filtration rates. Additionally, we detected the expression of genes related to cell chemotaxis such as *Syk* and *Ccl9*, which act as stimulators in the progression of DN[63,64], distinctly increased in the DKD group but were suppressed by RA. As expected, the results of DEP analysis further confirmed the damage-healing effect of RA on the DKD group.

Macrophages are considered as the principal cells involved in inflammatory regulation and their accumulation contributes to the severity of DN. There are two main phenotypes of macrophages namely M1 and M2, which are respectively recognized as accelerators and brakes for inflammation[65]. The S100a4+Mφ cells which are associated with the pro-inflammatory signaling (including TNF-α signaling by NF-κB and interferon gamma response) were significantly recruited in the DKD group, suggesting the involvement of these cells in the development of DN. TNF as regulators of NF-κB and ROS, promotes tissue-specific inflammatory injury[66]. Additionally, ROS-related genes, such as *Sod2*, *Hif1a* and *Prdx1*, were highly expressed in the activated S100a4+Mφ cells from our results. Notably, RA has been known for alleviating the symptoms of DN by inhibiting the generation of pro-inflammatory mediators and scavenging ROS[15,17].

As for lymphocytes, peripheral activated and infiltrating T and B cells are involved in the pathogenesis of DN and proteinuria[67,68]. Furthermore, NK cells have been proposed as important leukocytes infiltrating the kidney in glomerulonephritis models[69]. In instances of injury to tubular epithelial cells, there is an initial recruitment of NK cells to the kidney through the *TLR2-CCR5-CCL5* axis[70]. Our study revealed an increased proportion of T_C1, T_C2, and NK cells in DKD, with a subsequent decrease observed after RA treatment. The expression of *CCL5* was also restored as a result of RA treatment in our investigation. In contrast to T and B cells, NK cells exhibited higher cytotoxic and inflammatory response scores in our research. RA appears to regulate immune infiltration and inhibit the cytotoxicity of NK cells by reducing inflammatory responses during DN.

Dysfunction in intercellular crosstalk primarily involved in subtypes PT S1, Podo, Cd86+Mφ, S100a4+Mφ, and NK. Among these, M1-like macrophages Cd86+Mφ and S100a4+Mφ play central roles in altering cellular interactions, followed by NK cells. Ligand−receptor pairs involving immune suppressive genes such as *Cd274-Pdcd1* and *Cd86-Ctla4*, as well as those associated with pro-inflammatory responses such as *Ccl6-Ccr2* and *Ccl5-Ccr5*, are activated in DN and exhibit a decrease following RA treatment. Results from our analysis of intercellular communication suggest that RA might reduce intercellular crosstalk and remodel the cellular microenvironment in DN. In summary, our study investigated the cellular mechanism of RA treatment in DN, which is important for the future application of RA in treating DN. We identified some candidate biomarkers as diagnostic or additional therapeutic targets for the treatment of DN.

5. Conclusions

We employed single cell sequencing to profile transcriptomic changes of DKD model and RA treatment. Our results demonstrated that RA could ameliorate renal tubular epithelium injury, especially to the PT S1 and glomerular epithelial cells known as podocytes, and reduce oxidative stress and inflammation induced by DN. Furthermore, RA decreased the recruitment of S100a4 macrophages associated with pro-inflammatory signaling and remodeled the immune microenvironment during DN. Collectively, the study emphasizes the significance of RA in treating DN and proposes potential novel biomarkers for the diagnosis of DN.

Acknowledgments

This work was supported by the Establishment of Sino-Austria "Belt and Road" Joint Laboratory on Traditional Chinese Medicine for Severe Infectious Diseases and Joint Research (2020YFE0205100, China); National Key Research and Development Program of China (grant number 2020YFA0908000, 2022YFC2303600), the Innovation Team and Talents Cultivation Program of the National Administration of Traditional Chinese Medicine (grant number ZYYCXTD-C-202002, China), the National Natural Science Foundation of China (grant number 82074098, 81841001), the Fundamental Research Funds for the Central Public Welfare Research Institutes (grant number ZZ16-ND-10-23, ZZ15-ND-10, ZZ14-ND-010, ZZ14-FL-002, ZZ14-YQ-050, ZZ14-YQ-051, China), and Shenzhen Science and Technology Innovation Commission (grant number JCYJ20210324115800001 and JCYJ20210324114014039, China), the Shenzhen Medical Research Fund (B2302051, China), the Distinguished Expert Project of Sichuan Province Tianfu Scholar (CW202002, China), CACMS Innovation Fund (CI2023E002, CI2021A05101 and CI2021A05104, China) and support from State Key Laboratory for Quality Ensurance and Sustainable Use of Dao-di Herbs, Scientific and technological innovation project of China Academy of Chinese Medical Sciences (CI2023D003, CI2021B014, China).

Author contributions

Jigang Wang, Yulin Feng, Chunbo Chen, Sheng Nie, and Xinzhou Zhang contributed to design, concept, and supervise the project. Junhui Chen wrote the original manuscript. Qian Zhang, Jinan Guo, Di Gu, and Jing Liu revised and edited the manuscript. Jigang Wang and Yulin Feng reviewed and refined the manuscript. Qian Zhang, Jinan Guo, Di Gu, and Xinzhou Zhang provided and collected experimental material. Piao Luo and Qian Zhang constructed animal model and perfomed all experiments. Junhui Chen, Jing Liu, Yunmeng Bai and Jiayun Chen performed bioinformatics analysis. All authors participated in editing and reviewing the final manuscript

Conflicts of interest

The authors declare no competing or conflicts of interest in this research.

Appendix A. Supporting information

Supporting data to this article can be found online at https://doi.org/10.1016/j.apsb.2024.01.003.

References

1. Thomas MC, Cooper ME, Zimmet P. Changing epidemiology of type 2 diabetes mellitus and associated chronic kidney disease. *Nat Rev Nephrol* 2016;**12**:73−81.
2. Gheith O, Farouk N, Nampoory N, Halim MA, Al-Otaibi T. Diabetic kidney disease: world wide difference of prevalence and risk factors. *J Nephropharmacol* 2016;**5**:49−56.
3. Shu S, Krinock RA, Matsumura T, Sussman JJ, Fox BA, Chang AE, et al. Stimulation of tumor-draining lymph node cells with superantigenic staphylococcal toxins leads to the generation of tumor-specific effector T cells. *J Immunol* 1994;**152**:1277−88.
4. Selby NM, Taal MW. An updated overview of diabetic nephropathy: diagnosis, prognosis, treatment goals and latest guidelines. *Diabetes Obes Metabol* 2020;**22**(Suppl 1):3−15.
5. Vincent AM, Russell JW, Low P, Feldman EL. Oxidative stress in the pathogenesis of diabetic neuropathy. *Endocr Rev* 2004;**25**:612−28.
6. Matoba K, Takeda Y, Nagai Y, Kawanami D, Utsunomiya K, Nishimura R. Unraveling the role of inflammation in the pathogenesis of diabetic kidney disease. *Int J Mol Sci* 2019;**20**:3393.
7. Navarro-Gonzalez JF, Mora-Fernandez C, Muros de Fuentes M, Garcia-Perez J. Inflammatory molecules and pathways in the pathogenesis of diabetic nephropathy. *Nat Rev Nephrol* 2011;**7**:327−40.
8. Tesch GH. Macrophages and diabetic nephropathy. *Semin Nephrol* 2010;**30**:290−301.
9. Eisthen HL, Wysocki CJ, Beauchamp GK. Behavioral responses of male Guinea pigs to conspecific chemical signals following neonatal vomeronasal organ removal. *Physiol Behav* 1987;**41**:445−9.
10. Hitl M, Kladar N, Gavaric N, Bozin B. Rosmarinic acid-human pharmacokinetics and health benefits. *Planta Med* 2021;**87**:273−82.
11. Kim HK, Hwang S, Sung B, Kim YH, Chang Y. Gd-complex of a Rosmarinic acid conjugate as an anti-inflammatory theranostic agent *via* reactive oxygen species scavenging. *Antioxidants* 2020;**9**:744.
12. Ding Y, Zhang Z, Yue Z, Ding L, Zhou Y, Huang Z, et al. Rosmarinic acid ameliorates H_2O_2-induced oxidative stress in L02 cells through MAPK and Nrf2 Pathways. *Rejuvenation Res* 2019;**22**:289−98.
13. Luft JG, Steffens L, Moras AM, da Rosa MS, Leipnitz G, Regner GG, et al. Rosmarinic acid improves oxidative stress parameters and mitochondrial respiratory chain activity following 4-aminopyridine and picrotoxin-induced seizure in mice. *Naunyn-Schmiedeberg's Arch Pharmacol* 2019;**392**:1347−58.
14. Runtuwene J, Cheng KC, Asakawa A, Amitani H, Amitani M, Morinaga A, et al. Rosmarinic acid ameliorates hyperglycemia and insulin sensitivity in diabetic rats, potentially by modulating the expression of PEPCK and GLUT4. *Drug Des Dev Ther* 2016;**10**:2193−202.
15. Samsu N, Soeharto S, Rifai M, Rudijanto A. Rosmarinic acid monotherapy is better than the combination of rosmarinic acid and telmisartan in preventing podocyte detachment and inhibiting the progression of diabetic nephropathy in rats. *Biologics* 2019;**13**:179−90.
16. Aissa AF, Islam A, Ariss MM, Go CC, Rader AE, Conrardy RD, et al. Single-cell transcriptional changes associated with drug tolerance and response to combination therapies in cancer. *Nat Commun* 2021;**12**:1628.
17. Wu H, Gonzalez Villalobos R, Yao X, Reilly D, Chen T, Rankin M, et al. Mapping the single-cell transcriptomic response of murine diabetic kidney disease to therapies. *Cell Metabol* 2022;**34**:1064−1078 e1066.
18. Sun X, Zhou L, Wang Y, Deng G, Cao X, Ke B, et al. Single-cell analyses reveal cannabidiol rewires tumor microenvironment *via* inhibiting alternative activation of macrophage and synergizes with anti-PD-1 in colon cancer. *J Pharm Anal* 2023;**13**:726−44.
19. Chen J, He X, Bai Y, Liu J, Wong YK, Xie L, et al. Single-cell transcriptome analysis reveals the regulatory effects of artesunate on splenic immune cells in polymicrobial sepsis. *J Pharm Anal* 2023;**13**:817−29.
20. Deng G, Zhou L, Wang B, Sun X, Zhang Q, Chen H, et al. Targeting cathepsin B by cycloastragenol enhances antitumor immunity of CD8 T cells *via* inhibiting MHC-I degradation. *J Immunother Cancer* 2022;**10**:e004874.
21. Chen S, Zhou Y, Chen Y, Gu J. fastp: an ultra-fast all-in-one FASTQ preprocessor. *Bioinformatics* 2018;**34**:i884−90.
22. Hao Y, Hao S, Andersen-Nissen E, Mauck 3rd WM, Zheng S, Butler A, et al. Integrated analysis of multimodal single-cell data. *Cell* 2021;**184**:3573−3587 e3529.
23. Wu T, Hu E, Xu S, Chen M, Guo P, Dai Z, et al. clusterProfiler 4.0: a universal enrichment tool for interpreting omics data. *Innovation* 2021;**2**:100141.
24. Aibar S, Gonzalez-Blas CB, Moerman T, Huynh-Thu VA, Imrichova H, Hulselmans G, et al. SCENIC: single-cell regulatory network inference and clustering. *Nat Methods* 2017;**14**:1083−6.
25. Kumar N, Mishra B, Athar M, Mukhtar S. Inference of gene regulatory network from single-cell transcriptomic data using pySCENIC. *Methods Mol Biol* 2021;**2328**:171−82.
26. Jin S, Guerrero-Juarez CF, Zhang L, Chang I, Ramos R, Kuan CH, et al. Inference and analysis of cell-cell communication using CellChat. *Nat Commun* 2021;**12**:1088.
27. Kong W, Hui HWH, Peng H, Goh WWB. Dealing with missing values in proteomics data. *Proteomics* 2022;**22**:e2200092.
28. Ritchie ME, Phipson B, Wu D, Hu Y, Law CW, Shi W, et al. Limma powers differential expression analyses for RNA-sequencing and microarray studies. *Nucleic Acids Res* 2015;**43**:e47.
29. Strimmer K. fdrtool: a versatile R package for estimating local and tail area-based false discovery rates. *Bioinformatics* 2008;**24**:1461−2.
30. Xie Z, Bailey A, Kuleshov MV, Clarke DJB, Evangelista JE, Jenkins SL, et al. Gene set knowledge discovery with Enrichr. *Curr Protoc* 2021;**1**:e90.
31. Park J, Shrestha R, Qiu C, Kondo A, Huang S, Werth M, et al. Single-cell transcriptomics of the mouse kidney reveals potential cellular targets of kidney disease. *Science* 2018;**360**:758−63.
32. Lee JW, Chou CL, Knepper MA. Deep sequencing in microdissected renal tubules identifies nephron segment-specific transcriptomes. *J Am Soc Nephrol* 2015;**26**:2669−77.
33. Ho KM, Morgan DJR. The proximal tubule as the pathogenic and therapeutic target in acute kidney injury. *Nephron* 2022;**146**:494−502.
34. Chevalier RL. The proximal tubule is the primary target of injury and progression of kidney disease: role of the glomerulotubular junction. *Am J Physiol Ren Physiol* 2016;**311**:F145−61.

35. Fahal AH, Ibrahim A. Post-prostatectomy auto-irrigation with furosemide in the tropics. *Pharmatherapeutica* 1986;**4**:590−4.
36. Kirita Y, Wu H, Uchimura K, Wilson PC, Humphreys BD. Cell profiling of mouse acute kidney injury reveals conserved cellular responses to injury. *Proc Natl Acad Sci U S A* 2020;**117**:15874−83.
37. Rastaldi MP, Candiano G, Musante L, Bruschi M, Armelloni S, Rimoldi L, et al. Glomerular clusterin is associated with PKC-alpha/beta regulation and good outcome of membranous glomerulonephritis in humans. *Kidney Int* 2006;**70**:477−85.
38. Baelde HJ, Eikmans M, Doran PP, Lappin DW, de Heer E, Bruijn JA. Gene expression profiling in glomeruli from human kidneys with diabetic nephropathy. *Am J Kidney Dis* 2004;**43**:636−50.
39. Jia Y, Xu H, Yu Q, Tan L, Xiong Z. Identification and verification of vascular cell adhesion protein 1 as an immune-related hub gene associated with the tubulointerstitial injury in diabetic kidney disease. *Bioengineered* 2021;**12**:6655−73.
40. Nielsen SE, Schjoedt KJ, Astrup AS, Tarnow L, Lajer M, Hansen PR, et al. Neutrophil gelatinase-associated lipocalin (NGAL) and kidney injury molecule 1 (KIM1) in patients with diabetic nephropathy: a cross-sectional study and the effects of lisinopril. *Diabet Med* 2010;**27**:1144−50.
41. Morigi M, Perico L, Corna D, Locatelli M, Cassis P, Carminati CE, et al. C3a receptor blockade protects podocytes from injury in diabetic nephropathy. *JCI Insight* 2020;**5**:e131849.
42. Narita T, Hosoba M, Kakei M, Ito S. Increased urinary excretions of immunoglobulin g, ceruloplasmin, and transferrin predict development of microalbuminuria in patients with type 2 diabetes. *Diabetes Care* 2006;**29**:142−4.
43. Murray PJ, Wynn TA. Protective and pathogenic functions of macrophage subsets. *Nat Rev Immunol* 2011;**11**:723−37.
44. Geng XD, Wang WW, Feng Z, Liu R, Cheng XL, Shen WJ, et al. Identification of key genes and pathways in diabetic nephropathy by bioinformatics analysis. *J Diabetes Investig* 2019;**10**:972−84.
45. Eller K, Kirsch A, Wolf AM, Sopper S, Tagwerker A, Stanzl U, et al. Potential role of regulatory T cells in reversing obesity-linked insulin resistance and diabetic nephropathy. *Diabetes* 2011;**60**:2954−62.
46. Armingol E, Officer A, Harismendy O, Lewis NE. Deciphering cell−cell interactions and communication from gene expression. *Nat Rev Genet* 2021;**22**:71−88.
47. Buchbinder EI, Desai A. CTLA-4 and PD-1 pathways: similarities, differences, and implications of their inhibition. *Am J Clin Oncol* 2016;**39**:98−106.
48. Patsoukis N, Wang Q, Strauss L, Boussiotis VA. Revisiting the PD-1 pathway. *Sci Adv* 2020;**6**.
49. Imaoka M, Tanese K, Masugi Y, Hayashi M, Sakamoto M. Macrophage migration inhibitory factor-CD74 interaction regulates the expression of programmed cell death ligand 1 in melanoma cells. *Cancer Sci* 2019;**110**:2273−83.
50. Kong T, Ahn R, Yang K, Zhu X, Fu Z, Morin G, et al. CD44 Promotes PD-L1 expression and its tumor-intrinsic function in breast and lung cancers. *Cancer Res* 2020;**80**:444−57.
51. Palomino DC, Marti LC. Chemokines and immunity. *Einstein (Sao Paulo)* 2015;**13**:469−73.
52. Marinos E. Observations on the mitochondrial distribution in normal, rotated and cold-treated 2-cell stage embryos of Xenopus laevis. *Cell Differ* 1986;**18**:163−71.
53. Elmarakby AA, Sullivan JC. Relationship between oxidative stress and inflammatory cytokines in diabetic nephropathy. *Cardiovasc Ther* 2012;**30**:49−59.
54. Dziubla T, Butterfield DA. *Oxidative stress and biomaterials[M]*. Academic Press; 2016.
55. Hussain T, Tan B, Yin Y, Blachier F, Tossou MC, Rahu N. Oxidative stress and inflammation: what polyphenols can do for us? *Oxid Med Cell Longev* 2016;**2016**:7432797.
56. Hodgkins KS, Schnaper HW. Tubulointerstitial injury and the progression of chronic kidney disease. *Pediatr Nephrol* 2012;**27**:901−9.
57. Liu BC, Tang TT, Lv LL, Lan HY. Renal tubule injury: a driving force toward chronic kidney disease. *Kidney Int* 2018;**93**:568−79.
58. Zhuo JL, Li XC. Proximal nephron. *Compr Physiol* 2013;**3**:1079−123.
59. Ghezzi C, Yu AS, Hirayama BA, Kepe V, Liu J, Scafoglio C, et al. Dapagliflozin binds specifically to sodium-glucose cotransporter 2 in the proximal renal tubule. *J Am Soc Nephrol* 2017;**28**:802−10.
60. Duran-Salgado MB, Rubio-Guerra AF. Diabetic nephropathy and inflammation. *World J Diabetes* 2014;**5**:393−8.
61. Zhang Y, Lu X, Yang M, Shangguan J, Yin Y. GAS5 knockdown suppresses inflammation and oxidative stress induced by oxidized low-density lipoprotein in macrophages by sponging miR-135a. *Mol Cell Biochem* 2021;**476**:949−57.
62. Kravets I, Mallipattu SK. The role of podocytes and podocyte-associated biomarkers in diagnosis and treatment of diabetic kidney disease. *J Endocr Soc* 2020;**4**:bvaa029.
63. Zhang NN, Kang JS, Liu SS, Gu SM, Song ZP, Li FX, et al. Flavanomarein inhibits high glucose-stimulated epithelial-mesenchymal transition in HK-2 cells *via* targeting spleen tyrosine kinase. *Sci Rep* 2020;**10**:439.
64. Rojewska E, Zychowska M, Piotrowska A, Kreiner G, Nalepa I, Mika J. Involvement of macrophage inflammatory protein-1 family members in the development of diabetic neuropathy and their contribution to effectiveness of morphine. *Front Immunol* 2018;**9**:494.
65. Lopez-Parra V, Mallavia B, Egido J, Gomez-Guerrero C. Immunoinflammation in diabetic nephropathy: molecular mechanisms and therapeutic options. *Diabetic nephropathy* 2012:127−46.
66. Morgan MJ, Liu ZG. Crosstalk of reactive oxygen species and NF-kappaB signaling. *Cell Res* 2011;**21**:103−15.
67. Xiao X, Ma B, Dong B, Zhao P, Tai N, Chen L, et al. Cellular and humoral immune responses in the early stages of diabetic nephropathy in NOD mice. *J Autoimmun* 2009;**32**:85−93.
68. Ichinose K, Kawasaki E, Eguchi K. Recent advancement of understanding pathogenesis of type 1 diabetes and potential relevance to diabetic nephropathy. *Am J Nephrol* 2007;**27**:554−64.
69. Ikezumi Y, Kawachi H, Toyabe S, Uchiyama M, Shimizu F. An anti-CD5 monoclonal antibody ameliorates proteinuria and glomerular lesions in rat mesangioproliferative glomerulonephritis. *Kidney Int* 2000;**58**:100−14.
70. Kim HJ, Lee JS, Kim A, Koo S, Cha HJ, Han JA, et al. TLR2 signaling in tubular epithelial cells regulates NK cell recruitment in kidney ischemia-reperfusion injury. *J Immunol* 2013;**191**:2657−64.